Defective Ca^{2+}- dependent activation of TRPM4 channels contributes to age-related cerebral small vessel disease in *Col4a1* mutant mice

Evan Yamasaki[1], Pratish Thakore[1], Sher Ali[1], Alfredo Sanchez Solano[1], Xiaowei Wang[2], Xiao Gao[3,4], Cassandre Labelle-Dumais[2], Myriam M. Chaumeil[3,4], Douglas B. Gould[2,5], and Scott Earley[1*]

[1]Department of Pharmacology, Center for Molecular and Cellular Signaling in the Cardiovascular System, University of Nevada, Reno School of Medicine, Reno, NV 89557-0318, USA

[2]Department of Ophthalmology, UCSF School of Medicine, San Francisco, CA 94158, USA

[3]Department of Physical Therapy and Rehabilitation Science, UCSF School of Medicine, San Francisco, CA 94143, USA

[4]Department of Radiology and Biomedical Imaging, UCSF School of Medicine, San Francisco, CA 94143, USA

[5]Department of Anatomy, Institute for Human Genetics, Cardiovascular Research Institute, Bakar Aging Research Institute, UCSF School of Medicine, San Francisco, CA 94158, USA

Keywords: *COL4A1*, collagen, cerebral small vessel diseases, basement membrane, myogenic tone, TRPM4, IP_3R, Calcium, Ca^{2+}, ER Stress, SR Stress, ion channels.

[*]Corresponding author

Address Correspondence To: Scott Earley, Ph.D.
University of Nevada, Reno School of Medicine
Manville Health Sciences Building, Room 8
MS-0318
Reno, NV 89557-0318, USA
Phone: (775) 784-4117
Fax: (775) 784-1620
Email: searley@med.unr.edu

Abstract

Humans and mice with mutations in *COL4A1* and *COL4A2* manifest radiological and clinical hallmarks of cerebral small vessel disease (cSVD), but the pathogenic mechanisms are unknown. Here we report that mice with a missense mutation in *Col4a1* at amino acid 1344 (*Col4a1*$^{+/G1344D}$) exhibit age-dependent intracerebral hemorrhage (ICH), brain lesions detected by magnetic resonance imaging, and memory deficits. This pathology was associated with the loss of myogenic vasoconstriction, a vascular response essential for autoregulation of cerebral blood flow. Electrophysiological analyses showed that the loss of myogenic constriction resulted from blunted pressure-induced smooth muscle cell (SMC) membrane depolarization. Further, we found that dysregulation of membrane potential was associated with impaired Ca^{2+}-dependent activation of transient receptor potential melastatin 4 (TRPM4) cation channels and disruptions in sarcoplasmic reticulum (SR) Ca^{2+} signaling. Treating *Col4a1*$^{+/G1344D}$ mice with 4-phenylbutyrate, a compound that promotes the trafficking of misfolded proteins and alleviates SR stress, averted the loss of myogenic tone, prevented ICH, and reduced memory defects. We conclude that alterations in SR Ca^{2+} handling that impair TRPM4 channel activity results in dysregulation of SMC membrane potential and loss of myogenic tone which contributes to age-related cSVD in *Col4a1*$^{+/G1344D}$ mice.

Graphical Abstract

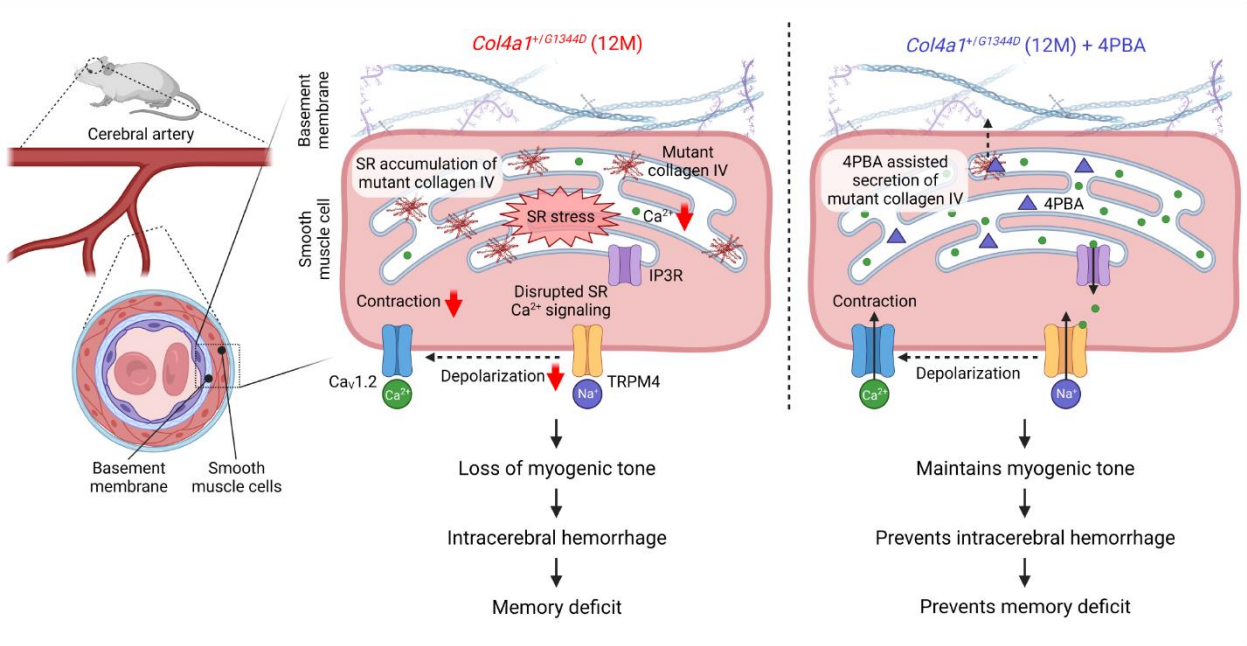

Introduction

Cerebral small vessel diseases (cSVDs) are a group of related pathologies that damage tiny arteries, arterioles, venules, and capillaries in the brain. These diseases are a major cause of stroke and, after Alzheimer's disease, the second leading cause of adult cognitive impairment and dementia (1, 2). The underlying pathogenic mechanisms of cSVDs remain largely unknown, and no specific treatment options exist. Sporadic and familial forms of cSVD share clinical and radiological features, including white matter hyperintensities, dilated perivascular spaces, lacunar infarcts, microbleeds, and intracerebral hemorrhages (ICHs) (3-6). Individuals with Gould syndrome, a rare multisystem disorder caused by autosomal dominant mutations in collagen IV alpha 1 (*COL4A1*) and alpha 2 (*COL4A2*), manifest these hallmarks of cSVD (7-9). The majority of pathogenic *COL4A1* and *COL4A2* mutations substitute critical glycine (G) residues within triple helical domains (10). These mutations impair the secretion of heterotrimers of COL4A1 and COL4A2 [$\alpha1\alpha1\alpha2$(IV)] which can lead to endoplasmic reticulum (ER) stress and/or disrupt the structure and function of basement membranes (11-13). However, it is not known how collagen defects and associated ER stress cause cSVD. An allelic series of *Col4a1* and *Col4a2* mutations demonstrate pathological heterogeneity (13). For the current study, we investigated the pathogenesis of *Col4a1*-associated cSVD using mice with a missense mutation that changes the G residue at amino acid position 1344 to aspartate (D). These animals, designated *Col4a1*$^{+/G1344D}$, model the most common type of mutation that occurs in humans and develop cSVD pathology that is more severe compared with others in the allelic series (10, 13).

Distinctive attributes of the cerebral vasculature serve the unique requirements of the brain. For example, cerebral arteries and arterioles exhibit graded constriction in response to changes in intravascular pressure. This vital autoregulatory process, known as the vascular myogenic response, protects downstream capillary beds from potentially harmful increases in perfusion pressure when cardiac output is elevated during exercise or other stimuli (14). The myogenic response is intrinsic to vascular smooth muscle cells (SMCs) and requires the coordinated activity of several ion channels. Increases in intraluminal pressure activate transient receptor potential melastatin 4 (TRPM4) channels, allowing an influx of Na^+ ions that depolarizes the plasma membrane to increase voltage-dependent Ca^{2+} inflow through Cav1.2 Ca^{2+} channels and engage the contractile apparatus (15, 16). Pressure-induced membrane depolarization is balanced by hyperpolarizing currents conducted by several K^+-permeable ion channels, including large-conductance Ca^{2+} activated K^+ (BK) channels, voltage-dependent K^+ (K_V) channels, and others (17-19). The interplay of depolarizing and hyperpolarizing currents controls the resting membrane potential of SMCs and maintains cerebral arteries in a state of partial contraction. BK and TRPM4 channels require high levels of intracellular Ca^{2+} for activation and, under native conditions, are stimulated by Ca^{2+} released from the sarcoplasmic reticulum (SR) through ryanodine receptors (RyRs) and inositol triphosphate receptors (IP_3Rs), respectively (17, 20). Impairment of the myogenic response has been implicated in many types of cerebrovascular disease, including familial cSVD associated with cerebral autosomal dominant arteriopathy with subcortical infarcts and leukoencephalopathy (CADASIL) caused by mutations in

NOTCH3 (21). However, the impact of *Col4a1* mutations on the myogenic response and how this affects neuronal pathology is not known.

Here, we report that *Col4a1*$^{+/G1344D}$ mice exhibit age-dependent loss of myogenic tone that is associated with spontaneous intracerebral hemorrhage (IHC), brain lesions detected by susceptibility-weighted magnetic resonance imaging (SWI), and defects in spatial working and recognition memory. The deficit in myogenic tone resulted from diminished stretch-induced activation of TRPM4 channels and impaired pressure-induced SMC membrane depolarization. We also found that subcellular and global Ca^{2+} signals generated by releasing Ca^{2+} from the SR through RyRs and IP_3Rs were disrupted in SMCs from aged *Col4a1*$^{+/G1344D}$ mice. Treating *Col4a1*$^{+/G1344D}$ mice with 4-phenylbutyrate (4PBA), a small molecule with chaperone properties that improves the secretion of misfolded proteins and diminishes ER/SR stress (10, 13, 22-25), attenuated the loss of myogenic tone, largely protected mice from ICH, and diminished memory deficits. These data suggest that SR stress in SMCs from *Col4a1*$^{+/G1344D}$ mice causes disruptions in intracellular Ca^{2+} signaling, stretch-induced activation of TRPM4 channels, pressure-induced SMC membrane potential depolarization, and myogenic constriction. Our data also suggest that these defects contribute to spontaneous ICH and memory defects. Thus, the findings of this study reveal a novel age-dependent mechanism of cSVD and identify 4PBA or other chaperone drugs as a potential treatment option.

Results

Col4a1$^{+/G1344D}$ mice exhibit age-dependent pathology

All studies utilized *Col4a1*$^{+/G1344D}$ mice or *Col4a1*$^{+/+}$ littermates as controls. Amino acid 1344 is part of a triple helical domain near the C-terminus (Figure 1A). To investigate age-related aspects of cSVD pathology, mice were studied at 3 and 12 months (M) of age, representing the young adult and middle-age stages of life, respectively. Male and female mice were used throughout the study, and no sex-specific differences were detected.

Spontaneous ICH is a highly penetrant and consequential manifestation of *Col4a1* mutations (26). ICH severity was measured in brain sections from *Col4a1*$^{+/+}$ and *Col4a1*$^{+/G1344D}$ mice stained with Prussian blue. In young adults, ICH was not detected in *Col4a1*$^{+/+}$ mice, but small punctate Prussian blue staining was present in brain sections from *Col4a1*$^{+/G1344D}$ mice (Figure 1B and C). Middle-aged *Col4a1*$^{+/+}$ mice did not exhibit ICH, but brain sections from 12 M-old *Col4a1*$^{+/G1344D}$ mice displayed large areas of Prussian blue staining mainly localized to the subcortical regions (Figure 1D and E). The total area of Prussian blue staining in 12 M-old *Col4a1*$^{+/G1344D}$ mice was nearly 20-fold more extensive than in 3 M-old mutants (1.9% vs. 0.1% of brain area, respectively), indicating that the severity of spontaneous ICH increases dramatically with age.

cSVDs are often diagnosed in individuals by radiological findings including brain lesions (27). Brain lesions were measured in 12 M-old *Col4a1*$^{+/+}$ and *Col4a1*$^{+/G1344D}$ mice *in vivo* using SWI. Middle-aged *Col4a1*$^{+/+}$ mice did not exhibit SWI-detectable brain

lesions, but brains from age-matched *Col4a1*$^{+/G1344D}$ mice had multiple lesions, mainly localized to the thalamus (Figure 1F-I). The number, total volume, and localization of brain lesions detected with SWI are consistent with ICH detected with Prussian blue staining.

Col4a1$^{+/G1344D}$ mice exhibit age-dependent declines in memory function

To evaluate the impact of *Col4a1* mutations on memory function, *Col4a1*$^{+/+}$ and *Col4a1*$^{+/G1344D}$ mice were subjected to the Y-maze spontaneous alternation behavioral assay (Figure 2A). This test was designed to detect defects in short-term spatial working memory (28). 3 M-old *Col4a1*$^{+/+}$ and *Col4a1*$^{+/G1344D}$ mice performed similarly in this test with no significant differences in spontaneous alternation, the maximum number of alternations, or total distance traveled (Figure 2B-D). In contrast, the alternation index of 12 M-old *Col4a1*$^{+/G1344D}$ mice was significantly reduced compared to age-matched *Col4a1*$^{+/+}$ animals (Figure 2E). There were no significant differences in the maximum number of alternations or distance moved (Figure 2F and G).

To test longer-term spatial reference memory, *Col4a1*$^{+/+}$ and *Col4a1*$^{+/G1344D}$ mice were subjected to the Y-maze novel arm behavioral assay (Figure 2H) (28). 3 M-old *Col4a1*$^{+/+}$ and *Col4a1*$^{+/G1344D}$ mice performed equally in this test, with no significant differences in the time spent or the number of entries in the novel arm (Figure 2I-K). However, the time spent and the number of entries in the novel arm of 12 M-old *Col4a1*$^{+/G1344D}$ mice was significantly lower than age-matched *Col4a1*$^{+/+}$ animals (Figure 2L-N). These data suggest that *Col4a1*$^{+/G1344D}$ mice exhibit age-dependent deficits in short-term and long-term memory.

Diminished pressure-induced constriction of cerebral arteries from middle-aged *Col4a1*$^{+/G1344D}$ mice is due to impaired SMC membrane depolarization.

To better understand the underlying causes of ICH and memory deficits in *Col4a1*$^{+/G1344D}$ mice, we used *ex vivo* pressure myography to study the myogenic response of cerebral arteries (29). Vasoconstriction in response to stepwise increases in intraluminal pressure (from 5 to 120 mmHg) was evaluated by measuring the active steady-state luminal diameter of cannulated cerebral arteries bathed in standard physiological saline solution at each pressure. This procedure was then repeated using a Ca^{2+}-free bathing solution to determine the passive response to pressure, and myogenic tone was calculated as the difference in active versus passive diameter normalized to the passive diameter. The myogenic tone of cerebral arteries isolated from 3 M-old *Col4a1*$^{+/+}$ and *Col4a1*$^{+/G1344D}$ mice did not differ (Figure 3A and B). However, cerebral arteries from 12 M-old *Col4a1*$^{+/G1344D}$ mice barely constricted in response to pressure and had significantly lower levels of myogenic tone than those from age-matched *Col4a1*$^{+/+}$ mice (Figure 3C and D). These data demonstrate that cerebral arteries from *Col4a1*$^{+/G1344D}$ mice lose myogenic tone with age.

SMCs in the vascular wall depolarize in response to increases in intraluminal pressure (30). Depolarization of the plasma membrane increases voltage-dependent Ca^{2+} influx to trigger muscular contraction and vasoconstriction (30, 31). To determine if the loss of myogenic tone in middle-aged *Col4a1*$^{+/G1344D}$ mice was associated with impaired pressure-induced depolarization, we recorded the membrane potentials of SMCs in intact cerebral arteries using intracellular microelectrodes. At a low intraluminal pressure (20 mmHg), the membrane potential of SMCs in cerebral arteries from 3 M-old

Col4a1$^{+/+}$ and *Col4a1*$^{+/G1344D}$ mice did not differ (Figure 3E and F). Increasing intraluminal pressure to physiological levels (80 mmHg) depolarized the SMC membrane potential in arteries from both groups to the same extent (Figure 3E and F). When vessels from 12 M-old animals were investigated, SMC membrane potential did not differ between *Col4a1*$^{+/+}$ and *Col4a1*$^{+/G1344D}$ when arteries were pressurized to 20 mmHg (Figure 3G and H). However, when intraluminal pressure was increased to 80 mmHg, the depolarization of SMCs in cerebral arteries from *Col4a1*$^{+/G1344D}$ mice was significantly blunted compared with controls (Figure 3G and H). These data suggest that cerebral arteries from 12 M-old *Col4a1*$^{+/G1344D}$ mice lose myogenic tone because pressure-induced SMC membrane depolarization is impaired.

Age-related declines in BK and TRPM4 channel activity in SMCs from *Col4a1*$^{+/G1344D}$ mice.

Changes in ion channel activity could account for impaired pressure-induced SMC depolarization in arteries from *Col4a1*$^{+/G1344D}$ mice. We used patch-clamp electrophysiology to compare the activity of hyperpolarizing K_V and BK channels and depolarizing TRPM4 channels in native SMCs from control and *Col4a1*$^{+/G1344D}$ mice.

Elevated SMC K_V channel current density is responsible for diminished myogenic tone in cerebral arteries from CADASIL cSVD mice (21). To determine if this mechanism accounts for the loss of myogenic tone in cerebral arteries from middle-aged *Col4a1*$^{+/G1344D}$ mice, we measured K_V currents in freshly isolated SMCs. K_V currents were recorded using the amphotericin B perforated patch-clamp configuration to maintain the integrity of intracellular signaling cascades. Whole-cell currents were evoked by applying voltage steps from -60 to +60 mV from a holding potential of -80 mV

in the presence of selective BK channel blocker paxilline (1 μM). The voltage step protocol was repeated in the presence of K_V channel blocker 4-aminopyridine (5 mM), and K_V current amplitude was determined at each potential by subtraction. We found that K_V current amplitudes did not differ between SMCs from 12 M-old *Col4a1*$^{+/+}$ and *Col4a1*$^{+/G1344D}$ mice at all applied command potentials (Supplemental Figure 1A and B).

The activity of BK channels in cerebral artery SMCs under native conditions is driven by the transient release of Ca^{2+} ions through RyRs on the SR into restricted subcellular microdomains proximal to the plasma membrane (32). These signaling events, known as Ca^{2+} sparks, activate clusters of BK channels on the plasma membrane to generate large-amplitude spontaneous transient outward currents (STOCs) (17, 18). We utilized the amphotericin B perforated patch-clamp configuration to measure STOCs in cerebral artery SMCs from 3 M-old *Col4a1*$^{+/+}$ and *Col4a1*$^{+/G1344D}$ mice over a range of command potentials (-60-0 mV) and saw no significant difference in STOC frequency or amplitude (Figure 4A-C). However, the frequency and amplitude of STOCs were significantly lower in cerebral artery SMCs from 12 M-old *Col4a1*$^{+/G1344D}$ mice compared with age-matched controls (Figure 4D-F). To determine if decreases in STOCs result from changes in gene expression, we utilized ddPCR to measure transcript levels of *Kcnma1* (BK subunit α), *Kcnmb1 (*BK subunit β1), and *Ryr2* (ryanodine receptor 2). No differences in mRNA expression levels were detected (Supplemental Figure 2).

Reduced BK channel activity depolarizes the SMC membrane potential and increases contractility (33). Thus, diminished BK channel activity in SMCs from 12 M-old

Col4a1$^{+/G1344D}$ mice cannot account for impaired pressure-induced membrane depolarization.

TRPM4 is a Ca^{2+}-activated, nonselective monovalent cation channel required for pressure-induced SMC depolarization and the development of myogenic tone in cerebral arteries (15, 16, 34, 35). Over the membrane potential range of SMCs in the vascular wall under physiological conditions (-60 to -30 mV), TRPM4 channels conduct inward Na^+ currents that depolarize the plasma membrane in response to increases in intraluminal pressure (15, 36). Patch-clamp electrophysiology was used to determine if TRPM4 activity is diminished in *Col4a1*$^{+/G1344D}$ mice. We assessed channel function and availability in freshly isolated cerebral artery SMCs using the conventional whole-cell patch-clamp configuration with a high [Ca^{2+}] intracellular solution to directly activate TRPM4. Currents were recorded as voltage ramps (-100 to +100 mV) were applied. Voltage ramps were repeated in the presence of TRPM4 blocker 9-phenanthrol (30 µM) (15), and TRPM4 currents were isolated by subtraction. Prior studies using ion substitution protocols have shown that Ca^{2+}-activated, 9-phenanthrol currents recorded using these methods are carried by Na^+ ions, providing substantial evidence that these are *bona fide* TRPM4 currents (16). We found that the amplitudes of whole-cell TRPM4 currents recorded from cerebral artery SMCs did not differ between *Col4a1*$^{+/+}$ and *Col4a1*$^{+/G1344D}$ mice at 3 and 12 M of age (Figure 4G-J). These data indicate that the collagen mutation studied here has no direct effects on TRPM4 channel function and does not impair the trafficking of channel protein to the plasma membrane.

TRPM4 channels in SMCs are activated by a signal transduction cascade initiated by angiotensin II type 1 receptors (AT_1Rs) (37-40). Activation of Gq protein-

coupled AT_1Rs stimulates phospholipase C (PLC), leading to the cleavage of phosphatidylinositol 4,5-bisphosphate (PIP_2) into diacylglycerol and inositol triphosphate (IP_3). IP_3 stimulates Ca^{2+} release from the SR through IP_3Rs to transiently activate TRPM4 channels (20, 35, 37). AT_1Rs are directly activated by the stretch of the plasma membrane in a manner independent of their ligand and are a critical mechanosensor in SMCs (37-40). To measure the activity of TRPM4 channels in response to mechanical force, we patch-clamped SMCs in the amphotericin B perforated patch configuration and applied negative pressure (-20 mmHg) through the patch pipet to stretch the plasma membrane. Stretch-induced transient inward cation currents (TICCs) evoked in this manner are blocked by 9-phenanthrol and abolished by knockdown of TRPM4 expression (15, 20). Stretch-activated TICC activity in SMCs from 3-M old *Col4a1*$^{+/+}$ and *Col4a1*$^{+/G1344D}$ (Figure 4K and L) did not differ. In contrast, stretch-induced TICC activity in SMCs from 12 M-old *Col4a1*$^{+/G1344D}$ mice was significantly lower than that of age-matched *Col4a1*$^{+/+}$ mice (Figure 4M and N). To determine if altered gene expression underlies the reduction in TICC activity, we utilized ddPCR to measure transcript levels of *Trpm4* (TRPM4), *Itpr1* (IP_3 receptor 1), and *Itpr2* (IP_3 receptor 2) in cerebral arteries from 12 M-old *Col4a1*$^{+/+}$ and *Col4a1*$^{+/G1344D}$ mice. No differences in mRNA copy number were observed (Supplemental Figure 2). These data suggest that blunted pressure-induced SMC depolarization and impaired myogenic tone result from diminished stretch-induced activation of TRPM4 channels.

Defective intracellular Ca^{2+} signaling in cerebral artery SMCs from middle-aged *Col4a1*$^{+/G1344D}$ mice.

Ca^{2+} released from the SR drives BK and TRPM4 channel activity in cerebral artery SMCs (17, 20). Therefore, we investigated the possibility that these vital SR Ca^{2+} signaling pathways are disrupted in SMCs from 12 M-old *Col4a1*$^{+/G1344D}$ mice. Freshly isolated SMCs were loaded with the Ca^{2+}-sensitive fluorophore Fluo-4 AM and imaged using high-speed, high-resolution spinning disk confocal microscopy. Spontaneous Ca^{2+} sparks were present in SMCs isolated from 3 M-old *Col4a1*$^{+/+}$ and *Col4a1*$^{+/G1344D}$ mice. The frequency, amplitude, duration, rise time, and decay rate did not differ between groups (Figure 5A-C). Spontaneous Ca^{2+} sparks were also present in SMCs isolated from both groups of middle-aged mice. No significant differences in Ca^{2+} spark amplitude, duration, rise time, and decay rate were observed, but notably, Ca^{2+} spark frequency was significantly lower in SMCs from 12 M-old *Col4a1*$^{+/G1344D}$ mice (Figure 4D-F). Diminished Ca^{2+} spark frequency likely accounts for decreased STOC frequency in SMCs from middle-aged *Col4a1* mutant mice.

Fluo-4 AM-loaded SMCs were challenged with a ryanodine receptor agonist, caffeine (10 mM), to investigate how RyR function was affected by the *Col4a1*$^{+/G1344D}$ mutation (41). Ca^{2+} signals arising from intracellular release were isolated from Ca^{2+} influx events by acutely removing Ca^{2+} from the extracellular solution immediately before recording. Caffeine-evoked global increases in cytosolic [Ca^{2+}] did not differ between SMCs from young adult *Col4a1*$^{+/+}$ and *Col4a1*$^{+/G1344D}$ mice (Figure 5G and H). In contrast, caffeine-induced global Ca^{2+} signals were smaller in amplitude in SMCs from 12 M-old *Col4a1*$^{+/G1344D}$ mice than in controls (Figure 5I and J). These data indicate that the release of SR Ca^{2+} from RyRs is impaired in the SMCs of *Col4a1*$^{+/G1344D}$ mice in an age-dependent manner.

Fluo-4 AM loaded-SMCs were also treated with the G_q protein-coupled thromboxane A2 receptor agonist U46619 to investigate IP_3R-mediated Ca^{2+} signaling. U46619-induced (100 nM) Ca^{2+} signals did not differ between cerebral artery SMCs from 3 M-old *Col4a1*$^{+/+}$ and *Col4a1*$^{+/G1344D}$ mice (Figure 5K and L). In contrast, Ca^{2+} signals induced by U46619 were smaller in amplitude in SMCs from 12 M-old *Col4a1*$^{+/G1344D}$ mice compared to controls (Figure 5M and N). These data suggest that the release of SR Ca^{2+} from IP_3Rs is also impaired in the SMCs of *Col4a1*$^{+/G1344D}$ mice in an age-dependent manner. RyRs and IP_3Rs share the same SR Ca^{2+} source (42). Impairment of Ca^{2+} release through both receptors suggests that the SR [Ca^{2+}] of SMCs from middle-aged *Col4a1*$^{+/G1344D}$ mice is lower than that of corresponding controls. Diminished SR Ca^{2+} levels could account for diminished STOC and TICC activity and decreased Ca^{2+} spark frequency.

4PBA prevents age-related loss of myogenic tone, spontaneous ICH, and spatial working memory deficits in *Col4a1*$^{+/G1344D}$ mice

Col4a1$^{+/G1344D}$ mice display increased intracellular accumulation of misfolded α1α1α2(IV) collagen, which causes ER/SR stress in collagen-producing cells (12, 13). The chemical chaperone 4PBA facilitates the trafficking of misfolded mutant proteins and reduces ER/SR stress (43). To investigate a potential link between impaired collagen secretion and the pathology of *Col4a1*$^{+/G1344D}$ mice, 4PBA (50 mM) was added to the drinking water of mutant and control animals from birth (postnatal day 0).

We found that age-related loss of myogenic tone was prevented by treating *Col4a1*$^{+/G1344D}$ mice with 4PBA (Figure 6A and B). Spontaneous ICH in middle-aged *Col4a1*$^{+/G1344D}$ mice treated with 4PBA was 4-fold lower than untreated *Col4a1*$^{+/G1344D}$

mice and did not differ from 4PBA-treated control mice (Figure 6C and D). These data suggest that 4PBA significantly diminishes the age-dependent myogenic tone defect and ICH in *Col4a1*$^{+/G1344D}$ mice. Finally, using the spontaneous alteration Y-maze assay, we found that although the mean alternation index of middle-aged *Col4a1*$^{+/G1344D}$ mice treated with 4PBA was slightly lower than 4PBA treated control mice, it was significantly higher than untreated *Col4a1*$^{+/G1344D}$ mice (Figure 6E). The maximum number of alternations and distance moved did not differ between 4PBA-treated 12 M-old *Col4a1*$^{+/G1344D}$ and *Col4a1*$^{+/+}$ and untreated *Col4a1*$^{+/G1344D}$ mice (Figure 6F and G). These data indicate that 4PBA treatment largely mitigates deficits in spatial working memory. We conclude that age-related loss of myogenic tone, ICH, and memory defects in *Col4a1*$^{+/G1344D}$ mice can be prevented or attenuated by treatment with 4PBA, linking the mutant's brain pathology with impaired secretion of misfolded collagen molecules and/or ER/SR stress.

Discussion

Despite the enormous impact of the disease, the molecular pathogenesis of cSVD is essentially unknown. Here we utilized the *Col4a1*$^{+/G1344D}$ mouse model of Gould syndrome to investigate how this monogenic form of cSVD damages small arteries in the brain during aging. Our findings show that these mice exhibit pathological changes with age that include the loss of myogenic tone, high levels of spontaneous ICH, brain lesions, and memory defects. Electrophysiology experiments revealed that the loss of myogenic tone is associated with diminished pressure-induced SMC depolarization and decreased activities of BK and TRPM4 channels. In addition, we found that fundamental RyR- and IP_3R-dependent Ca^{2+} signaling pathways are disrupted in SMCs from middle-aged *Col4a1*$^{+/G1344D}$ mice, likely due to a reduction in SR Ca^{2+} levels. Treating *Col4a1*$^{+/G1344D}$ mice with the chemical chaperone 4PBA negated the loss of myogenic tone, prevented spontaneous ICH, and reduced deficits in spatial working memory. We conclude that the age-dependent cSVD pathogenesis of *Col4a1*$^{+/G1344D}$ mice results from defects in SMC SR function that lead to reduced Ca^{2+} store load and disrupted intracellular Ca^{2+} signaling. Defects in subcellular Ca^{2+} signals diminish TRPM4 channel activity, disrupting membrane potential regulation and impeding pressure-induced constriction of cerebral arteries. These findings reveal a novel mechanism of age-dependent cSVD.

The myogenic response is a vital autoregulatory mechanism that protects delicate capillaries in the brain from pressure overload during increases in cardiac output and transient increases in perfusion associated with exercise, stress, and other stimuli (14). Loss of myogenic tone is observed in the CADASIL model of familial cSVD

(21, 44). Notably, Dabertrand *et al*. linked the loss of myogenic tone in the CADASIL model with blunted pressure-induced SMC membrane potential depolarization and connected the defect in membrane potential regulation with increased surface expression of K_V channels and elevated hyperpolarizing K^+ current density (21). Our study uncovered a different ion channel defect in the SMCs of *Col4a1*$^{+/G1344D}$ cSVD mice – Kv currents did not differ from controls but stretch-induced TRPM4 cation channel activity was greatly diminished. This defect was not due to reduced *Trpm4* expression, gross defects in channel function, or the number of channels available for activation on the plasma membrane. Instead, our data suggest that activation of TRPM4 by Ca^{2+} released from the SR through IP_3Rs was faulty in middle-aged *Col4a1*$^{+/G1344D}$ mice. The release of SR Ca^{2+} from RyRs was also impaired in SMCs from mutant mice, disrupting the Ca^{2+} spark – BK channel Ca^{2+} signaling pathway and diminishing STOC frequency. STOCs act as a negative feedback regulator to SMC pressure-induced membrane depolarization and contraction (45). However, because SMC pressure-induced membrane depolarization is impaired in middle-aged *Col4a1*$^{+/G1344D}$ mice, the STOC pathway is not engaged and has minimal influence on membrane potential. The impairment of multiple Ca^{2+} signaling modalities in mutant SMCs suggests that SR Ca^{2+} handling is defective. This concept is supported by a prior study showing that a ~16% decrease in SR [Ca^{2+}] diminished STOC frequency by 70% (46). Another study showed that depletion of SR [Ca^{2+}] to less than 80% of normal completely abolished IP_3R-mediated Ca^{2+} release (47). In many types of cells, store-operated Ca^{2+} entry (SOCE) is protective against decreases in ER/SR [Ca^{2+}] (48). However, SOCE is virtually undetectable in native, contractile vascular SMCs, promoting their susceptibility to

pathogenic SR Ca^{2+} depletion (49-51). We conclude that disrupted pressure-induced SMC depolarization and loss of myogenic tone in middle-aged *Col4a1*$^{+/G1344D}$ mice are due to impaired activation of TRPM4 by Ca^{2+} released from the SR.

Protein synthesis and folding occurs within the SR (52). *Col4a1*$^{+/G1344D}$ mice display impaired secretion and increased intracellular accumulation of collagen α1α1α2(IV), presumably due to the misfolding of mutant protein (13). Retention of misfolded proteins causes ER/SR stress (53). Our data showed that treatment with 4PBA, a molecular chaperone that promotes the secretion of misfolded proteins, prevented the loss of myogenic tone, attenuated spontaneous ICH, and diminished impairment of spatial working memory, suggesting that ER/SR stress contributes to the pathology of middle-aged *Col4a1*$^{+/G1344D}$ mice. One of the pathological manifestations of ER/SR stress is the depletion of Ca^{2+} stores (54). Yamato *et al.* (55) demonstrated that tunicamycin-induced ER stress promotes RyR-mediated ER Ca^{2+} leak, potentially due to increased reactive oxygen species (ROS) production that depleted ER Ca^{2+} store load. Steady-state free Ca^{2+} levels in the ER/SR are maintained by the release of Ca^{2+} into the cytosol through RyRs and IP_3Rs, mobile and stationary Ca^{2+}-binding proteins in the SR lumen, and transport of Ca^{2+} from the cytosol into the SR by sarco/endoplasmic reticulum ATPase (SERCA) enzymes (42), and any of these processes can be potentially impacted by ER/SR stress in *Col4a1*$^{+/G1344D}$ mice. Future investigations into possible links between SMC SR stress and Ca^{2+} handling defects in other genetic and sporadic forms of cSVD may reveal new therapeutic options.

This study showed that *Col4a1*$^{+/G1344D}$ mice display spontaneous ICH and memory deficits by middle age, reminiscent of the age-dependent effects of sporadic

cSVDs in humans. Our findings also indicate that dysregulation of critical SMC Ca^{2+} signaling mechanisms and TRPM4 channel activity is a central feature of cerebrovascular dysfunction in this model. The pathology of *Col4a1*$^{+/G1344D}$ mice is significantly attenuated by treatment with 4PBA, supporting the concept that promoting the secretion of misfolded proteins and/or reducing SR stress may be a viable treatment strategy for some forms of cSVD.

Materials and Methods

Chemical and reagents: All chemicals and other reagents were obtained from Sigma-Aldrich, Inc. (St. Louis, MO, USA) unless otherwise specified.

Animals: Young adult (3M) and middle-aged (12M) male and female littermate *Col4a1*$^{+/+}$ and *Col4a1*$^{+/G1344D}$ mice were used in this study. The *Col4a1*^{G1344D} mutation was backcrossed to C57BL/6J mice for over 20 generations (56). Animals were maintained in individually ventilated cages (≤5 mice/cage) with *ad libitum* access to food and water in a room with controlled 12-hour light and dark cycles. All animal care procedures and experimental protocols involving animals complied with the National Institutes of Health (NIH) *Guide for the Care and Use of Laboratory Animals* and were approved by the Institutional Animal Care and Use Committees at the University of Nevada, Reno, and University of California, San Francisco.

Histological analysis: Isoflurane anesthetized mice were transcardially perfused with ice-cold phosphate-buffered saline (PBS) followed by ice-cold 4% paraformaldehyde (Fisher, Waltham, MA, USA) in PBS. Brains were postfixed with 4% paraformaldehyde for 24 hours at 4°C, cryoprotected in 30% sucrose in PBS, and embedded in optimal cutting temperature compound (Fisher). Coronal cryosections (35 µm) regularly spaced (500 µm) along the rostrocaudal axis were stained with a Prussian blue and nuclear fast red stain kit (Abcam, Cambridge, UK) following the manufacture's protocol. Images were acquired with a BZ-X700 microscope using BZ-X Viewer 1.3.0.5 software and stitched with BZ-X Analyzer 1.3.0.3 software (Keyence, Osaka, Japan). The percentage of brain area with Prussian blue staining for each section was calculated with ImageJ

software (v2.3.0/1.53f; NIH, Bethesda, MD, USA). Hemorrhage severity was expressed as the average percentage of hemosiderin surface area on ~21 sections for each brain.

***In vivo* magnetic resonance imaging:** All *in vivo* magnetic resonance (MR) experiments were conducted on a 14.1 Tesla vertical MR system (Agilent Technologies, Palo-Alto, CA) equipped with 100 G/cm gradients and a single tuned millipede ^{1}H proton coil ($Ø_I$ = 40 mm). For each imaging session, mice were anesthetized using isoflurane (1-1.5% in O_2) and positioned in a dedicated craddle maintaining constant anesthesia and placed in the MR bore; respiration and temperature were continuously monitored during all acquisitions to ensure animal well-being and data reproducibility. Susceptibility weighted imaging (SWI) was performed to acquire high-resolution images of the mouse brain, using the following parameters: gradient-echo scheme, field of view (FOV) = 20 x 20 mm^2, matrix = 256 x 256, 16 slices, 0.4 mm slice thickness, 0.1 mm interslice gap, number of averages = 16, echo time (TE)/repetition time (TR) = 4.60/140ms, flip angle = 10 degrees. T2-weighted (T2W) images were also acquired in a fast-spin-echo scheme to evaluate brain anatomical structures, using the same FOV geometry as SWI and the following parameters: number of averages = 8, TE/TR = 21.38/2500ms, flip angle = 90 degrees. The fast-spin-echo based T2W imaging is less sensitive to distortion artifacts caused by B_0 inhomogeneity than SWI, and is thus used for the atlas-based brain structure registration as described below.

Hypointense lesions corresponding to ICH were quantified based on manual segmentation of the SWI images using an in-house software. To investigate the number of and distribution of hypointense SWI lesions across the brain, an open-sourced atlas-based imaging data analysis pipeline (AIDAmri) (57) was customized to register T2W

brain images to the Allen Brain Reference Atlas (58). Based on the registration result, the normalized lesion volumes for each brain region were summed up across all animals and an intra-group region-wise volumetric analysis was performed.

Y-Maze behavioral assessment: Memory function was assessed using the Y-maze (Maze Engineers, Skokie, IL, USA) using two different configurations.

The spontaneous alternation behavioral assay was used to assess short-term spatial working memory (28). Mice were placed into one of the three arms of maze (start arm) and were allowed to explore all three arms for 10 minutes. Session videos were recorded and analyzed using Ethovision XT software (version 16.0.1536, Noldus Information Technology, Leesburg, VA, USA). Spontaneous alternation was evaluated by scoring the order of entries into each arm during the 10-minute recording period. Spontaneous alternation was calculated as spontaneous alternation (%) = [number of spontaneous alternations/max alternation] $\times$ 100, where the spontaneous alternation is defined as the number consecutive entries into each arm of the maze in any order without any repeats, and the max alternation is the total number of alternations possible (max alternation = total number of arm entries – 2).

The novel arm configuration was used to evaluate longer-term spatial reference memory (28). This test was performed across 2 days. On day one, mice were placed into one of the three arms of maze (start arm) and were allowed to explore only two of the arms for 10 minutes (training trial). On day two, the test trial was conducted with the closed arm opened which served as the novel arm. Mice were returned into the maze via the same start arm and were allowed to explore all three arms for 10 minutes.

Session videos were recorded and analyzed using Ethovision XT software, and the time spent in the novel arm and entries into the novel arm were measured.

Isolation of cerebral arteries and SMCs: Mice were euthanized by decapitation under isoflurane anesthesia. Cerebral arteries were carefully isolated from the brain in Ca^{2+}-free Mg^{2+} physiological saline solution (Mg^{2+}-PSS) consisting of 140 mM NaCl, 5 mM KCl, 2 mM $MgCl_2$, 10 mM HEPES, and 10 mM glucose (pH 7.4, adjusted with NaOH), with 0.5% bovine serum albumin (BSA). Native SMCs for patch-clamp experiments were obtained by initially digesting isolated arteries in 1 mg/mL papain (Worthington Biochemical Corporation, Lakewood, NJ, USA), 1 mg/mL dithiothreitol (DTT), and 10 mg/mL BSA in Ca^{2+}-free PSS at 37°C for 12 minutes, followed by a 14-minute incubation with 1 mg/mL type II collagenase (Worthington Biochemical Corporation). A single-cell suspension was prepared by washing digested arteries three times with Mg^{2+}-PSS and triturating with a fire-polished glass pipette. All cells used for this study were freshly dissociated on the day of experimentation.

Pressure myography: The current best practices guidelines for pressure myography experiments were followed (29). Arteries were mounted between two glass cannulas (outer diameter, 40–50 μm) in a pressure myograph chamber (Living Systems Instrumentation, St Albans City, VT, USA) and secured by a nylon thread. Intraluminal pressure was controlled using a servo-controlled peristaltic pump (Living Systems Instrumentation), and preparations were visualized with an inverted microscope (Accu-Scope Inc., Commack, NY, USA) coupled to a USB camera (The Imaging Source LLC, Charlotte, NC, USA). Changes in luminal diameter were assessed using IonWizard software (version 7.2.7.138; IonOptix LLC, Westwood, MA, USA). Arteries were bathed

in warmed (37°C), oxygenated (21% O_2, 6% CO_2, 73% N_2) PSS (119 mM NaCl, 4.7 mM KCl, 21 mM $NaHCO_3$, 1.17 mM $MgSO_4$, 1.8 mM $CaCl_2$, 1.18 mM KH_2PO_4, 5 mM glucose, 0.03 mM EDTA) at an intraluminal pressure of 5 mmHg. Following equilibration for 15 min, intraluminal pressure was increased to 110 mmHg, and vessels were stretched to their approximate *in vivo* length, after which pressure was reduced back to 5 mmHg for an additional 15 min. Vessel viability was assessed for each preparation by evaluating vasoconstriction response to high extracellular [K^+] PSS, made isotonic by adjusting the [NaCl] (60 mM KCl, 63.7 mM NaCl). Arteries that showed less than 10% constriction in response to elevated [K^+] were excluded from further investigation.

Myogenic tone was assessed by raising the intraluminal pressure stepwise from 5 mmHg to 120 mmHg in 20 mmHg increments (5-20 mmHg for the first step). The active diameter was obtained by allowing vessels to equilibrate for at least 5 minutes at each pressure or until a steady-state diameter was reached. Following completion of the pressure-response study, intraluminal pressure was lowered to 5 mmHg, and arteries were superfused with Ca^{2+}-free PSS supplemented with EGTA (2 mM) and the voltage-dependent Ca^{2+} channel blocker diltiazem (10 μM) to inhibit SMC contraction, after which passive diameter was obtained by repeating the stepwise increase in intraluminal pressure. Myogenic tone at each pressure step was calculated as myogenic tone (%) = [1 – (active lumen diameter/passive lumen diameter)] $\times$ 100.

Membrane potential: For measurements of SMC membrane potential, cerebral arteries were isolated, cannulated, and viability confirmed as described. SMC membrane potential was recorded from intact pressurized arteries at intraluminal pressures of 20

mmHg and 80 mmHg. SMCs were impaled through the adventitia with glass intracellular microelectrodes (100-200 MΩ) backfilled with 3M KCl. Membrane potential was recorded using an Electro 705 amplifier (World Precision Instruments, Sarasota, FL, USA). Analog output from the amplifier was recorded using Ionwizard software (version 7.5.1.162; IonOptix). Criteria for acceptance of membrane potential recordings were 1) an abrupt negative deflection of potential as the microelectrode was advanced into a cell; 2) stable membrane potential for at least 30 seconds, and 3) an abrupt change in the potential to ~0 mV after the electrode was retracted from the cell.

Electrophysiological recordings: Enzymatically-isolated native SMCs were transferred to a recording chamber (Warner Instruments, Holliston, MA, USA) and allowed to adhere to glass coverslips for 20 minutes at room temperature. Recording electrodes (3–5 MΩ) were pulled on a model P-87 micropipette puller (Sutter Instruments, Novato, CA, USA) and polished using a MF-830 MicroForge (Narishige Scientific Instruments Laboratories, Long Island, NY, USA). Currents were recorded at room temperature using an Axopatch 200B amplifier (Molecular Devices, Sunnyvale, CA, USA) equipped with an Axon CV 203BU headstage and Digidata 144A digitizer (Molecular Devices) for all patch-clamp electrophysiology experiments. Clampex and Clampfit (version 10.2; Molecular Devices) were used for data acquisition and analysis.

The bathing solution composition for perforated-patch recordings of Kv currents, STOCs, and TICCs was 134 mM NaCl, 6 mM KCl, 1 mM $MgCl_2$, 2 mM $CaCl_2$, 10 mM HEPES, and 10 mM glucose (pH 7.4, adjusted with NaOH). The patch pipette solution contained 110 mM K-aspartate, 1 mM $MgCl_2$, 30 mM KCl, 10 mM NaCl, 10 mM HEPES, and 5 μM EGTA (pH 7.2, adjusted with KOH). Amphotericin B (200 μM) was included in

the pipette solution to gain electrical access. Whole-cell K^+ currents were recorded using a step protocol (-60 to +60 mV in 10 mV, 250 ms steps) from a holding potential of -80 mV. The BK channel blocker paxilline (1 µM) was included in the bath solution when Kv currents were recorded. Whole-cell K^+ currents were recorded in the absence and presence of K_V channel blocker 4-aminopyridine (5 mM), and the Kv component was determined by subtraction. Summary current-voltage (I-V) plots were generated using values obtained from the last 50 ms of each step. STOCs were recorded from SMCs voltage-clamped over a range of membrane potentials (-60 to 0 mV; 10 mV steps). TICCs were recorded from SMCs voltage-clamped at -70 mV; membrane stretch was delivered by applying negative pressure through the recording electrode using a pressure clamp system (HSPC-1; ALA Scientific Instruments Inc., Farmingdale, NY, USA). TICC activity was calculated as the sum of the open channel probability (NP_o) of multiple open states of 1.75 pA (59).

Whole-cell TRPM4 currents were recorded in a bath solution consisting of 156 mM NaCl, 1.5 mM $CaCl_2$, 10 mM glucose, 10 mM HEPES, and 10 mM TEACl (pH 7.4, adjusted with NaOH). The patch pipette solution contained 156 mM CsCl, 8 mM NaCl, 1 mM $MgCl_2$, 10 mM HEPES (pH 7.4, adjusted with NaOH), and a free Ca^{2+} concentration of 200 µM, adjusted using the appropriate amount of $CaCl_2$ and EGTA, as determined with Max-Chelator software (WEBMAXC standard, available at https://somapp.ucdmc.ucdavis.edu/pharmacology/bers/maxchelator/webmaxc/webmaxcS.htm. Whole-cell cation currents were evoked by applying 400 ms voltage ramps from -100 to +100 mV from a holding potential of -60 mV. Voltage ramps were repeated every 2 s for 300 s. The selective TRPM4 inhibitor 9-phenanthrol (30 µM) was applied after

peak TRPM4 current was recorded (~100 s). Whole-cell TRPM4 current amplitude was expressed as the 9-phenanthrol-sensitive current at +100 mV.

Quantitative droplet digital PCR: Total RNA was extracted from isolated cerebral arteries by homogenization in TRIzol reagent (Invitrogen, Waltham, MA, USA), followed by purification using a Direct-zol RNA microprep kit (Zymo Research, Irvine, CA, USA) with on-column DNAse treatment. RNA concentration was determined using an RNA 6000 Pico Kit run on a Bioanalyzer 2100 running Agilent 2100 Expert Software (B.02.11; Agilent Technologies, Santa Clara, CA, USA). RNA was converted to cDNA using iScript cDNA Supermix (Bio-Rad, Hercules, CA, USA). Quantitative droplet digital PCR (ddPCR) was performed using QX200 ddPCR EvaGreen Supermix (Bio-Rad), custom-designed primers (Supplementary Table 1), and cDNA templates. Generated droplet emulsions were amplified using a C100 Touch Thermal Cycler (Bio-Rad), and the fluorescence intensity of individual droplets were measured using a QX200 Droplet Reader (Bio-Rad) running QuantaSoft (version 1.7.4; Bio-Rad). Analysis was performed using QuantaSoft Analysis Pro (version 1.0596; Bio-Rad).

Ca^{2+} imaging: Images were acquired using an iXon 897 EMCCD camera (Andor; 16 × 16 µm pixel size) coupled to a spinning-disk confocal head (CSU-X1; Yokogawa) with a 100× oil-immersion objective (Olympus; NA 1.45) at an acquisition rate of 33 frames per second (fps). Custom software (SparkAn; https://github.com/vesselman/SparkAn) provided by Dr. Adrian D. Bonev (University of Vermont) was used to analyze the properties of Ca^{2+} sparks and whole-cell RyR and IP_3R Ca^{2+} signals.

To image Ca^{2+} sparks, a suspension of freshly isolated SMCs was placed in a glass-bottom 35 mm dish, and cells were allowed to adhere to the glass coverslip for 20 min

at room temperature. SMCs were then loaded with the Ca^{2+}-sensitive fluorophore, Fluo-4-AM (1 µM; Invitrogen), in the dark for 20 minutes at room temperature in Mg^{2+}-PSS. Cells were subsequently washed three times with Ca^{2+}-containing PSS and incubated at room temperature for 20 min in the dark to allow sufficient time for Fluo-4 de-esterification. The threshold for Ca^{2+} spark detection was defined as local increases in fluorescence ≥0.2 $\Delta F/F_0$.

To image RyR and IP_3R Ca^{2+} signals, SMCs were plated and loaded with Fluo-4-AM as stated above, but immediately before imaging, cells were washed three times and imaged in Mg^{2+}-PSS to eliminate signals resulting from the influx of Ca^{2+}. Caffeine (10 mM) or U46619 (100 nM; Enzo Biochem, Farmingdale, NY) were applied to the bath.

4PBA treatment: Mice were provided with 4-phenylbutyrate (4PBA; 50 mM; Scandinavian Formulas Inc., Sellersville, PA, USA) from birth in drinking water that was refreshed weekly as described previously (25).

Statistical analysis: All summary data are presented as means ± SEM. Statistical analyses were performed, and graphs were constructed using Prism version 9.3.1 (GraphPad Software, San Diego, CA, USA). The value of n refers to the number of cells for patch-clamp electrophysiology and Ca^{2+} imaging experiments, number of arteries for pressure myography and membrane potential experiments, and number of animals for histological analyses, magnetic resonance imaging, Y-maze, and ddPCR experiments. Statistical analyses were performed using unpaired Student's t-tests and one-way and two-way analysis of variance (ANOVA). A P value < 0.05 was considered statistically significant for all analyses.

Grant support: This study was supported by grants from the National Institutes of Health (NHLBI R35HL155008, R01HL091905, R01HL137852, R01HL139585, R01146054 and R01HL122770, and NIGMS P20GM130459 to S.E. and NINDS RF1NS110044 and R33NS115132 to M.M.C, D.B.G, and S.E. ; The Transgenic Genotyping and Phenotyping Core at the COBRE Center for Molecular and Cellular Signaling in the Cardiovascular System, University of Nevada, Reno, is maintained by a grant from NIH/NIGMS (P20GM130459 Sub#5451), as is the High Spatial and Temporal Resolution Imaging Core at the COBRE Center for Molecular and Cellular Signaling in the Cardiovascular System, University of Nevada, Reno (P20GM130459 Sub#5452). The UCSF Department of Ophthalmology is supported by P30EY002162 and an unrestricted grant from Research to Prevent Blindness.

Author contributions: S.E. and D.B.G. initiated and supervised the project. S.E. designed the experiments. E.Y. performed brain histology, pressure myography, sharp electrode and patch-clamp electrophysiology, Ca^{2+} imaging, and ddPCR experiments. X.W. and X.G. performed magnetic resonance imaging experiments. S.A. and A.S.S. performed patch-clamp electrophysiology experiments. P.T. performed pressure myography and Y-maze experiments. C.L.D. performed animal colony management. E.Y., S.A., A.S.S., P.T., X.G., and S.E. analyzed the data. E.Y. and S.E. drafted the manuscript and prepared the figures. E.Y., C.L.D, M.M.C., D.B.G., and S.E. revised the manuscript.

Competing interests: The authors declare that they have no competing interests.

Data and materials availability: All data needed to evaluate the conclusions in the paper are present in the paper or the Supplementary Materials

Figures

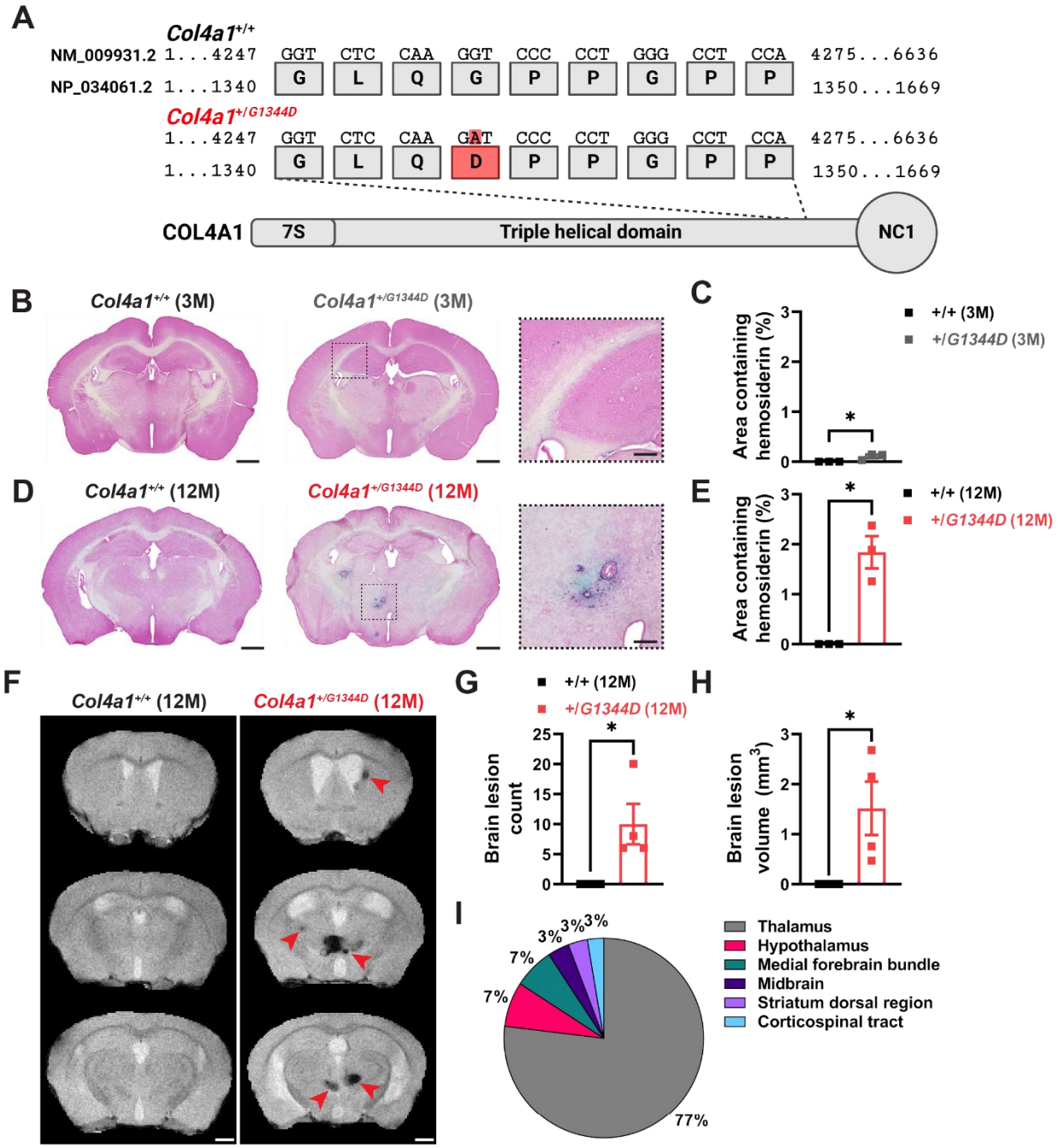

Figure 1. *Col4a1*$^{+/G1344D}$ mice exhibit age-dependent pathologies. (A) Schematic representation of the *Col4a1* point mutation that leads to *Col4a1*^{G1344D}. **(B)** Intracerebral hemorrhage (ICH) was assessed using Prussian blue staining. Representative images

of brain sections from 3M-old *Col4a1*$^{+/+}$ and *Col4a1*$^{+/G1344D}$ mice stained with Prussian blue. **(C)** Summary data presented as percentage of brain area with Prussian blue staining in brain sections (500 µm intervals). N = 3 animals per group. *P ≤ 0.05, unpaired t-test. **(D)** Representative images of brain sections from 12 M-old *Col4a1*$^{+/+}$ and *Col4a1*$^{+/G1344D}$ mice stained with Prussian blue. **(E)** Summary data presented as percentage of brain area with Prussian blue staining in brain sections (500 µm intervals). N = 3 animals per group. *P ≤ 0.05, unpaired t-test. **(F)** Brain lesions were evaluated *in vivo* using high field susceptibility-weighted magnetic resonance imaging (SWI). Representative SWI images from 12M-old *Col4a1*$^{+/+}$ and *Col4a1*$^{+/G1344D}$ mice. Red arrow heads highlight hypointense pixels that indicate hemorrhagic lesions. Quantification of **(G)** the number of lesions and **(H)** the total volume of lesions detected by SWI. N = 4 animals per group. *P ≤ 0.05, unpaired t-test. **(I)** Region-wise volumetric distribution of lesions detected by SWI from 12M-old *Col4a1*$^{+/G1344D}$ mice. Scale bars = 1 mm. Inset scale bars = 250 µm.

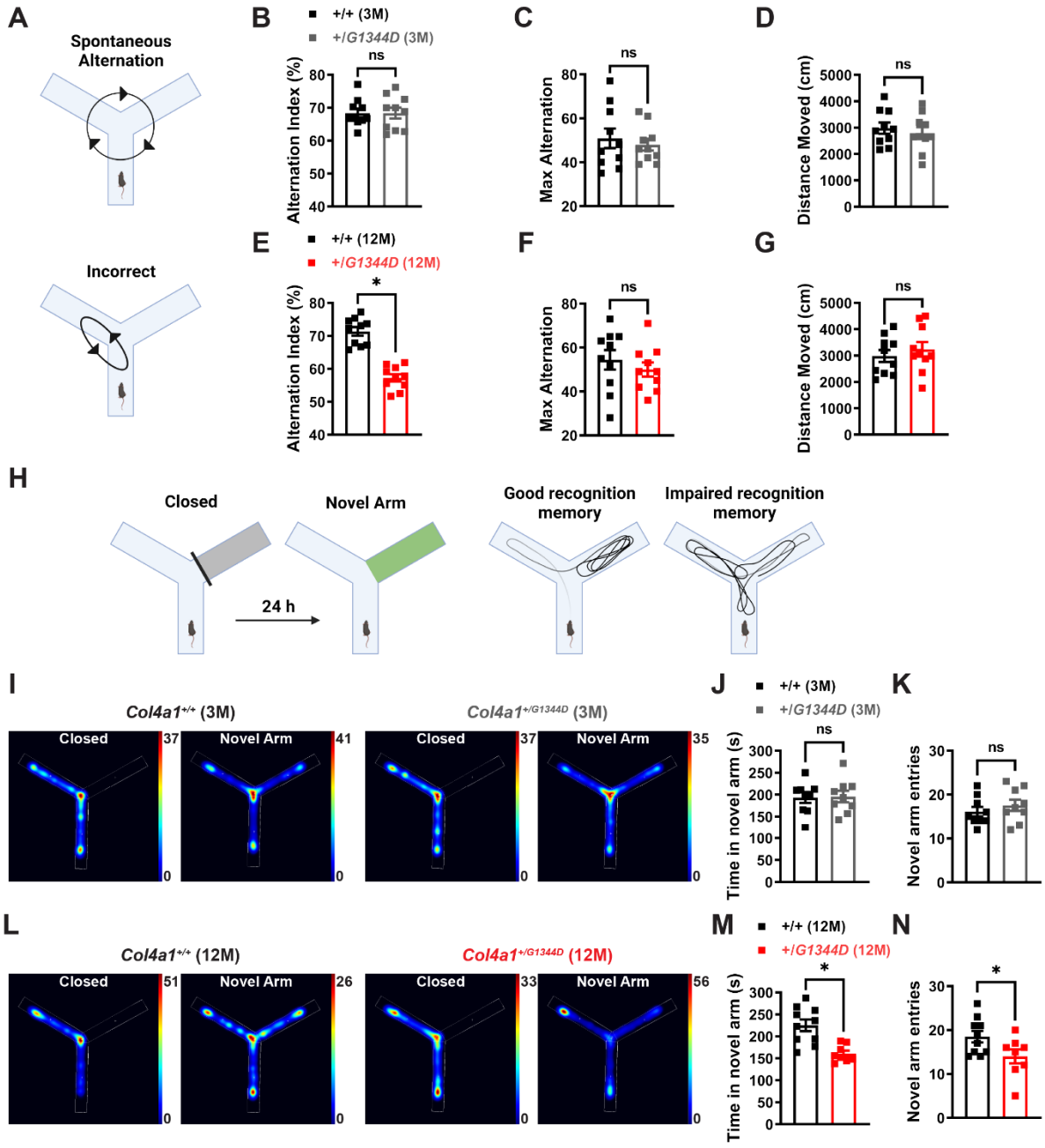

Figure 2. *Col4a1*$^{+/G1344D}$ mice have age-dependent decline in memory function. (A) Illustration of Y-maze spontaneous alternation behavior assay showing examples of a correct (top) and incorrect (bottom) spontaneous alternation. Summary data of **(B)** alternation index, **(C)** max number of alternations reflecting exploratory activity, and **(D)** total distance moved during spontaneous alternation Y-maze task of 3 M-old *Col4a1*$^{+/+}$

and *Col4a1*$^{+/G1344D}$ mice. N = 10 animals per group. ns = not significant, unpaired t-test. **(E)** Summary data of alternation index, **(F)** max number of alternations, and **(G)** total distance moved during spontaneous alternation Y-maze task of 12 M-old *Col4a1*$^{+/+}$ and *Col4a1*$^{+/G1344D}$ mice. N =10 animals per group. *P ≤ 0.05, ns = not significant, unpaired t-test. **(H)** Illustration of Y-maze novel arm procedure. **(I)** Heatmaps showing the time (s) that 3 M-old *Col4a1*$^{+/+}$ and *Col4a1*$^{+/G1344D}$ mice spent in areas of the Y-maze during the novel arm assay. **(J)** Summary data of dwell time and **(K)** entries into the novel arm. N = 9 animals per group. ns = not significant, unpaired t-test. **(L)** Heatmaps showing the time (s) that 12 M-old *Col4a1*$^{+/+}$ and *Col4a1*$^{+/G1344D}$ mice spent in areas of the Y-maze during the novel arm assay. **(M)** Summary data of dwell time and **(N)** entries into the novel arm. N = 8 or 10 animals per group. *P ≤ 0.05, unpaired t-test.

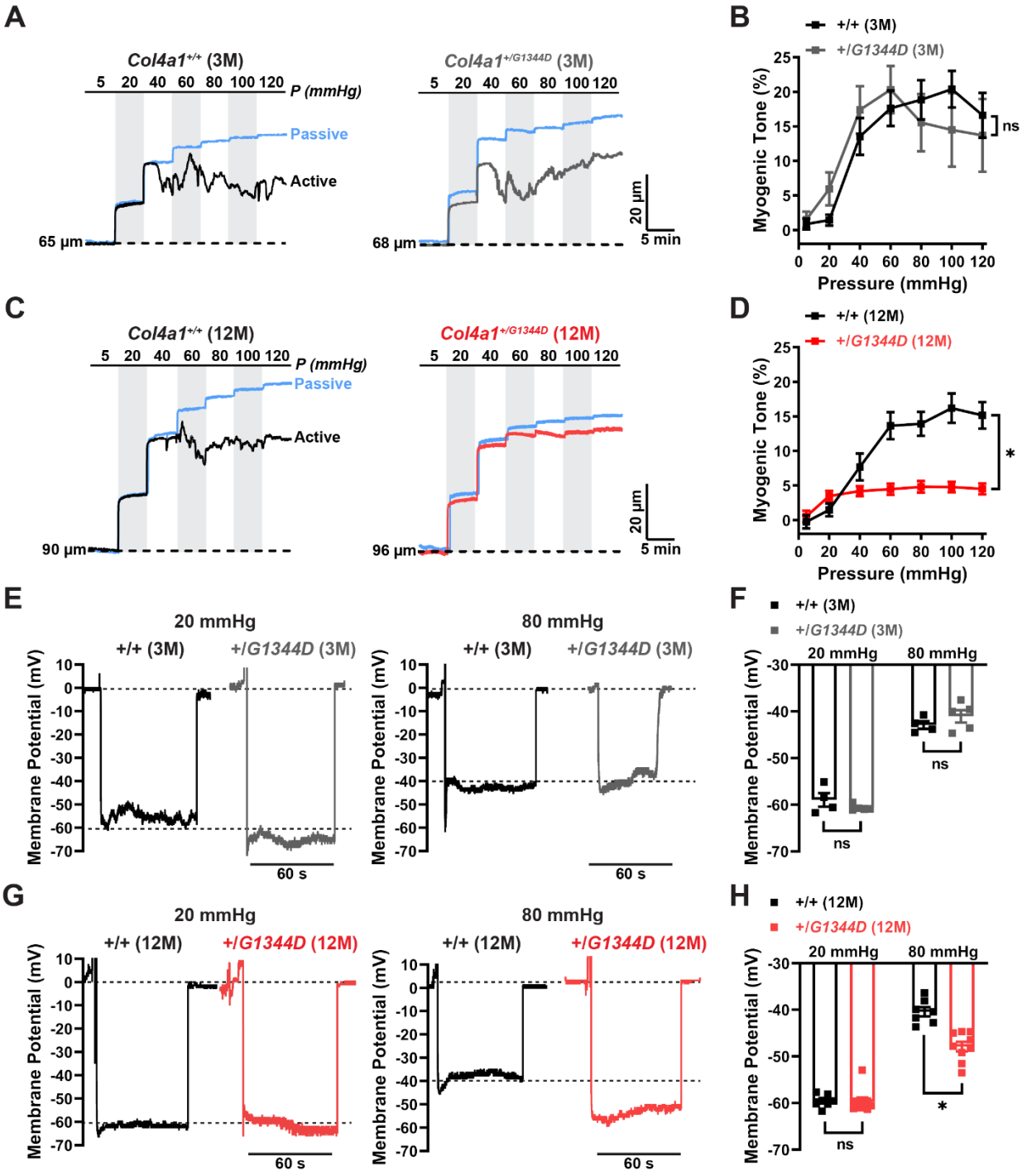

Figure 3. Cerebral arteries from *Col4a1*$^{+/G1344D}$ mice have age-dependent loss of myogenic tone and pressure induced depolarization. (A) Representative recordings of the inner diameter of isolated cerebral arteries from 3 M-old *Col4a1*$^{+/+}$ and

Col4a1$^{+/G1344D}$ mice showing the myogenic response to increases in pressure (active) and the dilation of the same arteries when extracellular Ca^{2+} has been removed (passive). **(B)** Summary data of myogenic tone as a function of intraluminal pressure. n = 5-10 vessels from 5 or 6 animals per group. ns = not significant, two-way ANOVA. **(C)** Representative recordings of the inner diameter of isolated cerebral arteries from 12 M-old *Col4a1*$^{+/+}$ and *Col4a1*$^{+/G1344D}$ mice. **(D)** Summary data of myogenic tone as a function of intraluminal pressure. n = 13 vessels from 6 or 9 animals per group. *P ≤ 0.05, two-way ANOVA. **(E)** Representative membrane potential (mV) recordings of smooth muscle cells (SMCs) in pressurized cerebral arteries isolated from 3 M-old *Col4a1*$^{+/+}$ and *Col4a1*$^{+/G1344D}$ mice at 20 mmHg and 80 mmHg intraluminal pressure. **(F)** Summary data showing membrane potential of SMCs in pressurized cerebral arteries at 20 mmHg and 80 mmHg intraluminal pressure. n = 4-5 vessels from 3 or 4 animals per group. ns = not significant, unpaired t-test. **(G)** Representative membrane potential recordings of SMCs in pressurized cerebral arteries isolated from 12 M-old *Col4a1*$^{+/+}$ and *Col4a1*$^{+/G1344D}$ mice at 20 mmHg and 80 mmHg intraluminal pressure. **(H)** Summary data showing membrane potential of SMCs in pressurized cerebral arteries at 20 mmHg and 80 mmHg intraluminal pressure. n = 7-9 vessels from 5 or 6 mice per group. *P ≤ 0.05, unpaired t-test.

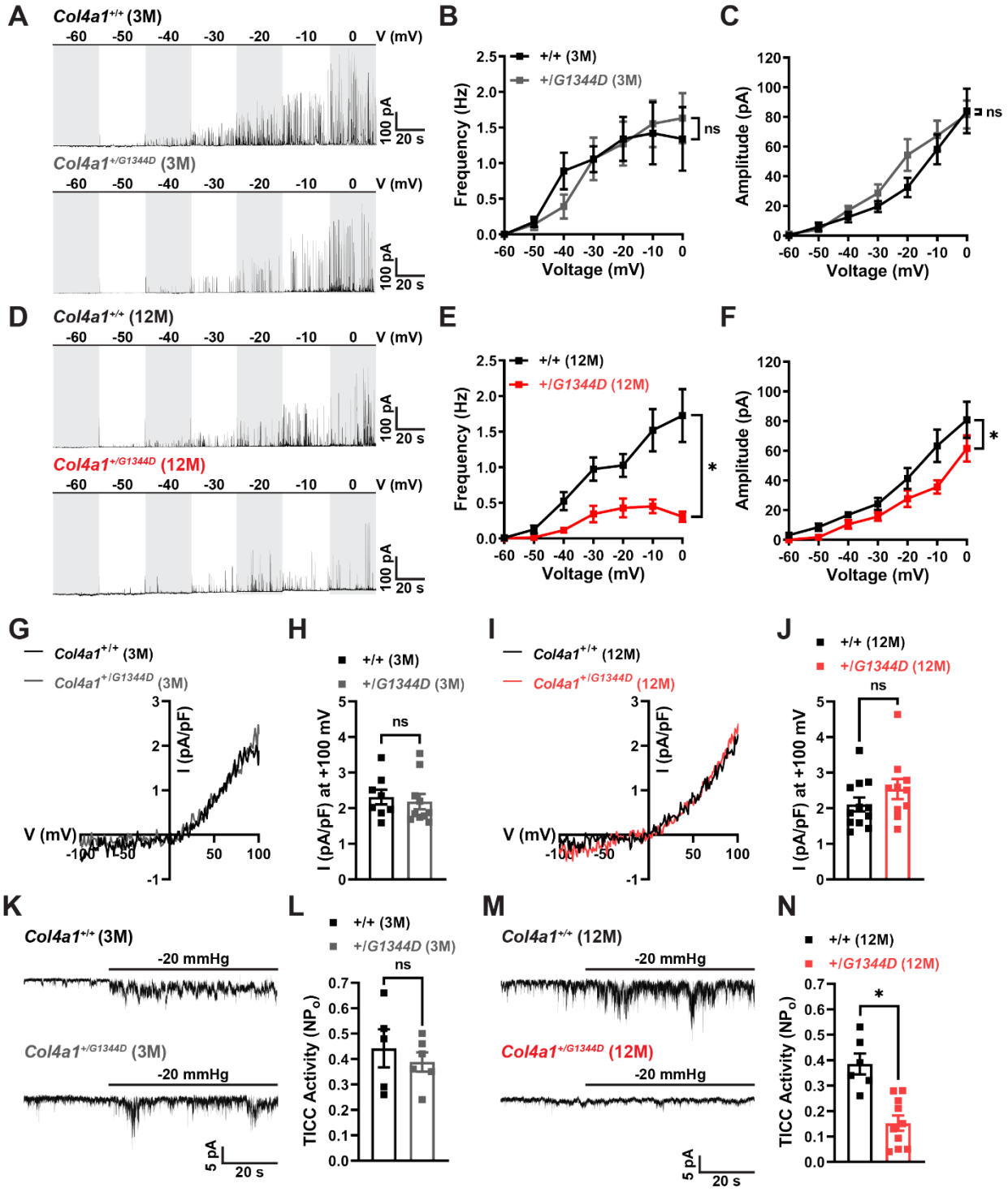

Figure 4. Age-dependent decrease in physiological BK and TRPM4 channel activity in *Col4a1*$^{+/G1344D}$ mice. (A) Representative traces of spontaneous transient outward currents (STOCs) in freshy isolated cerebral artery smooth muscle cells

(SMCs) from 3 M-old *Col4a1*$^{+/+}$ and *Col4a1*$^{+/G1344D}$ mice over a range of membrane potentials (-60 to 0 mV). Summary data showing STOC frequency **(B)** and amplitude **(C)** at each command potential. n = 8-12 cells from 5 animals per group. ns = not significant, two-way ANOVA. **(D)** Representative traces of STOCs in cerebral artery SMCs from 12 M-old *Col4a1*$^{+/+}$ and *Col4a1*$^{+/G1344D}$ mice. Summary data showing STOC frequency **(E)** and amplitude **(F)** at each command potential. n = 12 cells from 5 animals per group. *P ≤ 0.05, two-way ANOVA. **(G)** Representative I-V plots of whole-cell patch-clamp TRPM4 current recordings during voltage ramps (-100 to 100 mV) in cerebral artery SMCs from 3 M-old *Col4a1*$^{+/+}$ and *Col4a1*$^{+/G1344D}$ mice. Currents were evoked by including 200 µM free Ca^{2+} in the intracellular solution and the TRPM4 portion of the current was determined with the addition of TRPM4 blocker 9-phenanthrol (30 µM). **(H)** Summary of whole-cell TRPM4 current density at +100 mV. n = 8-10 cells from 3 or 4 animals per group. ns = not significant, unpaired t-test. **(I)** Representative I-V plots of whole-cell patch-clamp TRPM4 current recordings in cerebral artery SMCs from 12 M-old *Col4a1*$^{+/+}$ and *Col4a1*$^{+/G1344D}$ mice. **(J)** Summary of whole-cell TRPM4 current density at +100 mV. n = 10-12 cells from 4 animals per group. ns = not significant, unpaired t-test. **(K)** Representative traces of transient inward cation currents (TICCs) evoked by applying negative pressure (-20 mmHg) to stretch the plasma membrane of voltage-clamped (-70 mV) cerebral artery SMCs isolated from 3 M-old *Col4a1*$^{+/+}$ and *Col4a1*$^{+/G1344D}$ mice. **(L)** Summary data of TICC activity. n = 5-6 cells from 3 animals per group. ns = not significant, unpaired t-test. **(M)** Representative traces of TICCs in cerebral artery SMCs isolated from 12 M-old *Col4a1*$^{+/+}$ and *Col4a1*$^{+/G1344D}$ mice. **(N)**

Summary data of TICC activity. n = 8-10 cells from 4 or 5 animals per group. *P ≤ 0.05, unpaired t-test.

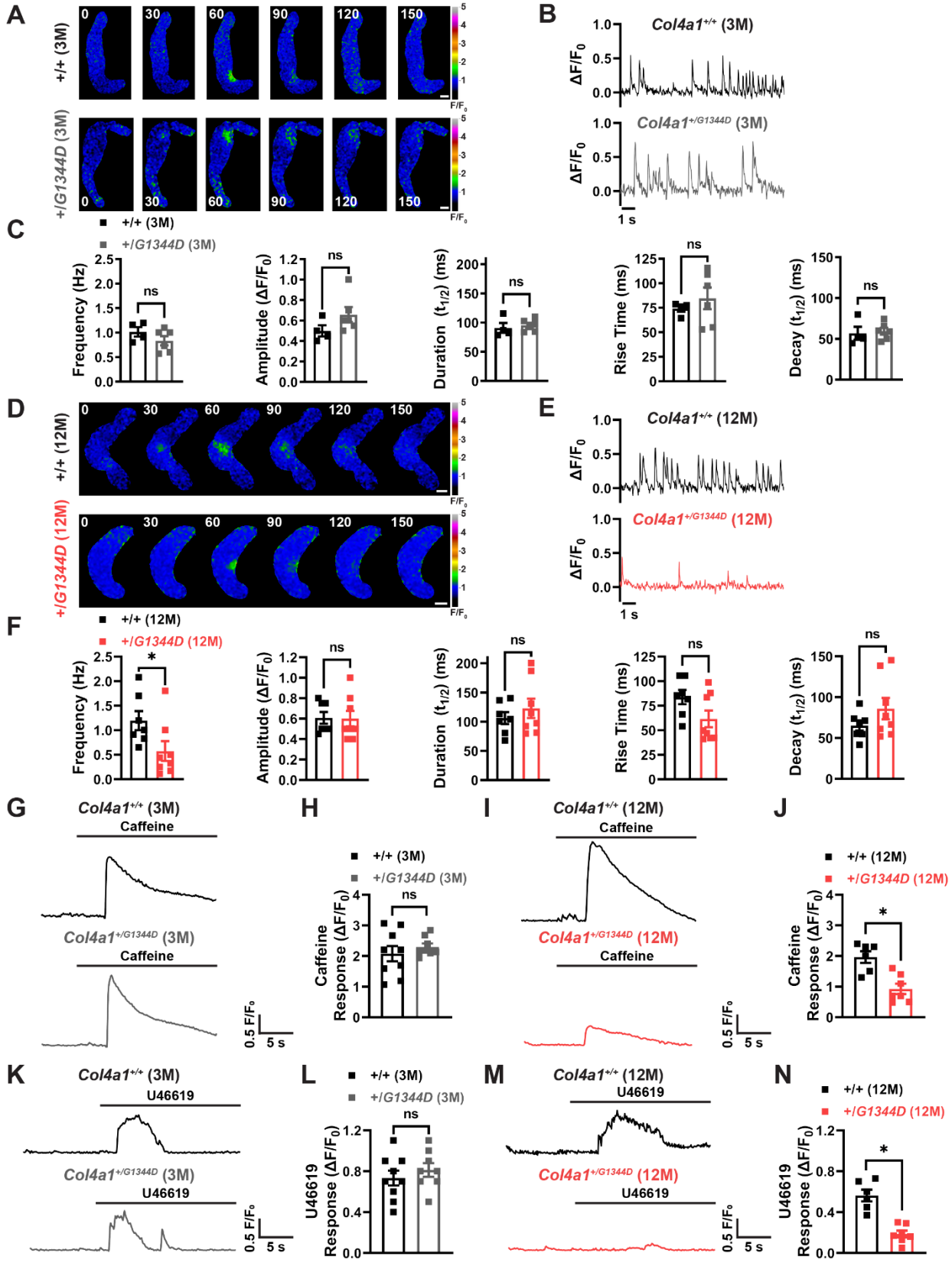
A
+/+ (3M)
+/G1344D (3M)
0
30
60
90
120
150
F/F0
B
Col4a1+/+ (3M)
Col4a1+/G1344D (3M)
ΔF/F0
1 s
C
+/+ (3M)
+/G1344D (3M)
Frequency (Hz)
Amplitude (ΔF/F0)
Duration (t1/2) (ms)
Rise Time (ms)
Decay (t1/2) (ms)
ns
D
+/+ (12M)
+/G1344D (12M)
E
Col4a1+/+ (12M)
Col4a1+/G1344D (12M)
F
+/+ (12M)
+/G1344D (12M)
*
G
Col4a1+/+ (3M)
Caffeine
Col4a1+/G1344D (3M)
0.5 F/F0
5 s
H
Caffeine Response (ΔF/F0)
I
Col4a1+/+ (12M)
Col4a1+/G1344D (12M)
J
K
U46619
L
U46619 Response (ΔF/F0)
M
N

Figure 5. *Col4a1*$^{+/G1344D}$ mice have altered sarcoplasmic reticulum Ca^{2+} signaling. **(A)** Representative time-course spinning disk confocal images exhibiting Ca^{2+} spark events in Fluo-4-AM loaded cerebral artery smooth muscle cells (SMCs) from 3 M-old *Col4a1*$^{+/+}$ and *Col4a1*$^{+/G1344D}$ mice. Time = milliseconds, scale bar = 5 µm. **(B)** Representative traces of Ca^{2+} spark events in cerebral artery SMCs isolated from 3 M-old *Col4a1*$^{+/+}$ and *Col4a1*$^{+/G1344D}$ mice presented as changes in fractional fluorescence ($\Delta F/F_0$) vs. time. **(C)** Summary data showing Ca^{2+} spark frequency, amplitude, duration, rise time, and decay. n = 4-6 cells from 3 animals per group. ns = not significant, unpaired t-test. **(D)** Representative time-course images exhibiting Ca^{2+} spark events in cerebral artery SMCs from 12 M-old *Col4a1*$^{+/+}$ and *Col4a1*$^{+/G1344D}$. Time = milliseconds, scale bar = 5 µm. **(E)** Representative traces of Ca^{2+} spark events in cerebral artery SMCs isolated from 12 M-old *Col4a1*$^{+/+}$ and *Col4a1*$^{+/G1344D}$ mice presented $\Delta F/F_0$ vs. time. **(F)** Summary data showing Ca^{2+} spark frequency, amplitude, duration, rise time, and decay. n = 7-8 cells from 3 or 4 animals per group. *$P \leq 0.05$, ns = not significant, unpaired t-test. **(G)** Representative traces showing whole cell changes in F/F_0 in response to caffeine (10 mM) in Fluo-4-AM loaded cerebral artery SMCs from 3 M-old *Col4a1*$^{+/+}$ and *Col4a1*$^{+/G1344D}$ mice. **(H)** Summary data of the $\Delta F/F_0$ in response to caffeine. n = 8-9 cells from 3 animals per group. ns = not significant, unpaired t-test. **(I)** Representative traces showing whole cell changes in F/F_0 in response to caffeine in SMCs from 12 M-old *Col4a1*$^{+/+}$ and *Col4a1*$^{+/G1344D}$ mice. **(J)** Summary data of the $\Delta F/F_0$ in response to caffeine. n = 6-7 cells from 3 animals per group. *$P \leq 0.05$, unpaired t-test. **(K)** Representative traces showing whole cell changes in F/F_0 in response to U46619 (100 nM) in Fluo-4-AM loaded cerebral artery SMCs from 3 M-old *Col4a1*$^{+/+}$

and *Col4a1*$^{+/G1344D}$ mice. **(L)** Summary data of the $\Delta F/F_0$ in response to U46619. n = 8-9 cells from 3 animals per group. ns = not significant, unpaired t-test. **(M)** Representative traces showing whole cell changes in F/F_0 in response to U46619 in SMCs from 12 M-old *Col4a1*$^{+/+}$ and *Col4a1*$^{+/G1344D}$ mice. **(N)** Summary data of the $\Delta F/F_0$ in response to U46619. n = 6-7 cells from 3 animals per group. *$P \leq 0.05$, unpaired t-test.

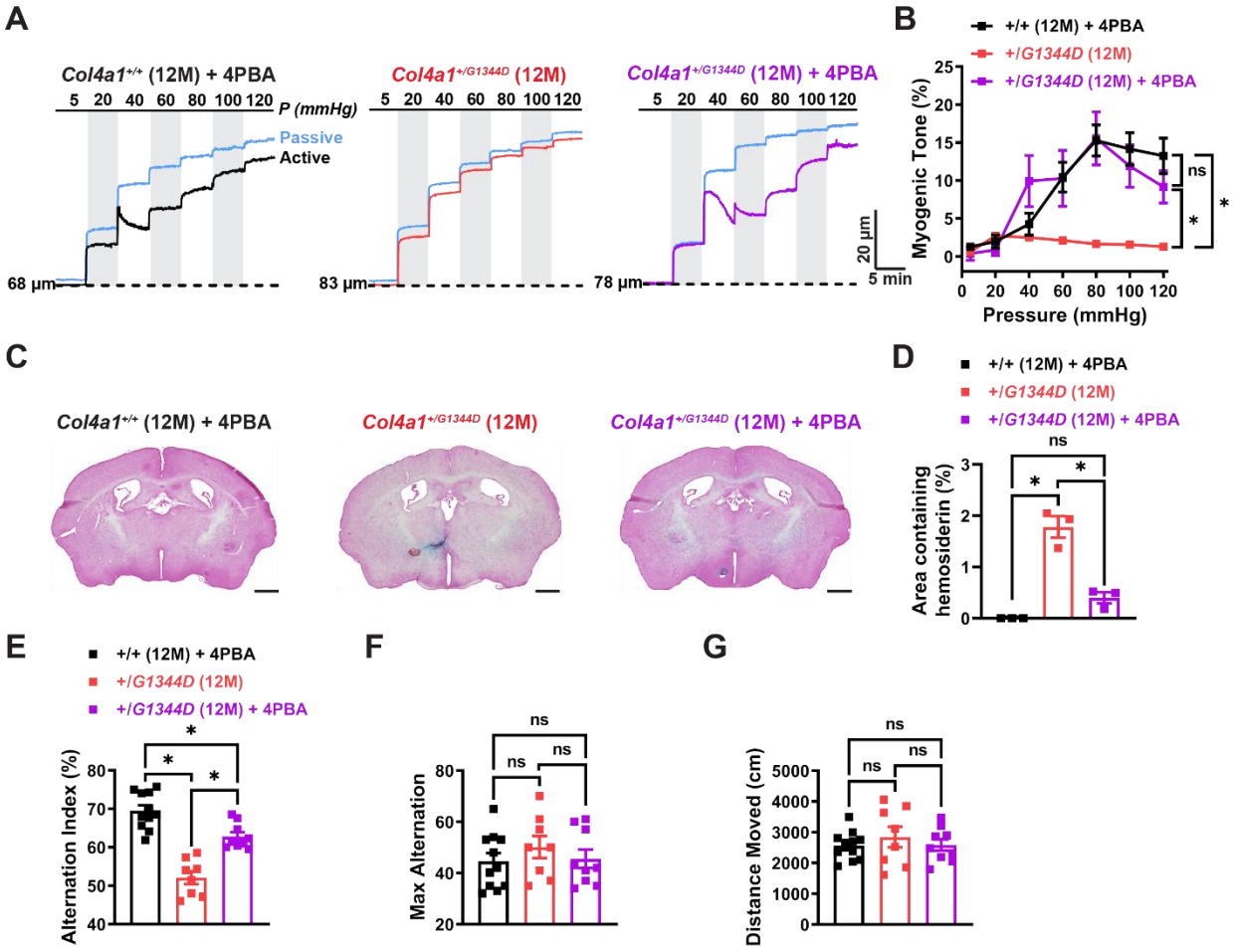

Figure 6. 4PBA prevents age-related cerebrovascular dysfunction. **(A)** Representative recordings of the inner diameter of isolated cerebral arteries from 4PBA treated 12 M-old *Col4a1*$^{+/+}$ and *Col4a1*$^{+/G1344D}$ and untreated *Col4a1*$^{+/G1344D}$ mice showing the myogenic response to increases in pressure (active) and the dilation of the same arteries when extracellular Ca^{2+} has been removed (passive). **(B)** Summary data of myogenic tone as a function of intraluminal pressure. n = 6 or 9 vessels from 3 or 5 mice. *P ≤ 0.05, ns = not significant, two-way ANOVA. **(C)** Representative images of Prussian blue stained brain sections from 4PBA treated 12 M-old *Col4a1*$^{+/+}$ and *Col4a1*$^{+/G1344D}$ and untreated *Col4a1*$^{+/G1344D}$ mice. Scale bar = 1 mm. **(D)** Summary data presented as percentage of brain area with Prussian blue staining in brain sections (500

µm intervals). N = 3 animals per group. *P ≤ 0.05, ns = not significant, one-way ANOVA. Short-term spatial working memory of 4PBA treated 12 M-old *Col4a1*$^{+/+}$ and *Col4a1*$^{+/G1344D}$ mice and untreated *Col4a1*$^{+/G1344D}$ mice was assessed by spontaneous alternation in the Y-maze; **(E)** summary data of alternation index, **(F)** max number of alternations reflecting exploratory activity, and **(G)** total distance moved during spontaneous alternation Y-maze task. N = 9, 8, or 11 animals per group. *P ≤ 0.05, ns = not significant one-way ANOVA.

References Cited

1. Markus HS. Genes, endothelial function and cerebral small vessel disease in man. *Exp Physiol.* 2008;93(1):121-7.
2. Pantoni L. Cerebral small vessel disease: from pathogenesis and clinical characteristics to therapeutic challenges. *Lancet Neurol.* 2010;9(7):689-701.
3. Choi JC. Genetics of cerebral small vessel disease. *J Stroke.* 2015;17(1):7-16.
4. Joutel A, and Faraci FM. Cerebral small vessel disease: insights and opportunities from mouse models of collagen IV-related small vessel disease and cerebral autosomal dominant arteriopathy with subcortical infarcts and leukoencephalopathy. *Stroke.* 2014;45(4):1215-21.
5. Joutel A, Haddad I, Ratelade J, and Nelson MT. Perturbations of the cerebrovascular matrisome: A convergent mechanism in small vessel disease of the brain? *J Cereb Blood Flow Metab.* 2016;36(1):143-57.
6. Rutten-Jacobs LC, Traylor M, Adib-Samii P, Thijs V, Sudlow C, Rothwell PM, et al. Common NOTCH3 Variants and Cerebral Small-Vessel Disease. *Stroke.* 2015;46(6):1482-7.
7. Gould DB, Phalan FC, Breedveld GJ, van Mil SE, Smith RS, Schimenti JC, et al. Mutations in Col4a1 cause perinatal cerebral hemorrhage and porencephaly. *Science.* 2005;308(5725):1167-71.
8. Gould DB, Phalan FC, van Mil SE, Sundberg JP, Vahedi K, Massin P, et al. Role of COL4A1 in small-vessel disease and hemorrhagic stroke. *N Engl J Med.* 2006;354(14):1489-96.
9. Lanfranconi S, and Markus HS. COL4A1 mutations as a monogenic cause of cerebral small vessel disease: a systematic review. *Stroke.* 2010;41(8):e513-8.
10. Jeanne M, Jorgensen J, and Gould DB. Molecular and Genetic Analyses of Collagen Type IV Mutant Mouse Models of Spontaneous Intracerebral Hemorrhage Identify Mechanisms for Stroke Prevention. *Circulation.* 2015;131(18):1555-65.
11. Jeanne M, Labelle-Dumais C, Jorgensen J, Kauffman WB, Mancini GM, Favor J, et al. COL4A2 mutations impair COL4A1 and COL4A2 secretion and cause hemorrhagic stroke. *Am J Hum Genet.* 2012;90(1):91-101.
12. Gould DB, Marchant JK, Savinova OV, Smith RS, and John SW. Col4a1 mutation causes endoplasmic reticulum stress and genetically modifiable ocular dysgenesis. *Hum Mol Genet.* 2007;16(7):798-807.
13. Kuo DS, Labelle-Dumais C, Mao M, Jeanne M, Kauffman WB, Allen J, et al. Allelic heterogeneity contributes to variability in ocular dysgenesis, myopathy and brain malformations caused by Col4a1 and Col4a2 mutations. *Hum Mol Genet.* 2014;23(7):1709-22.
14. Davis MJ, and Hill MA. Signaling mechanisms underlying the vascular myogenic response. *Physiol Rev.* 1999;79(2):387-423.
15. Gonzales AL, Garcia ZI, Amberg GC, and Earley S. Pharmacological inhibition of TRPM4 hyperpolarizes vascular smooth muscle. *Am J Physiol Cell Physiol.* 2010;299(5):C1195-202.

16. Earley S, Waldron BJ, and Brayden JE. Critical role for transient receptor potential channel TRPM4 in myogenic constriction of cerebral arteries. *Circ Res.* 2004;95(9):922-9.
17. Nelson MT, Cheng H, Rubart M, Santana LF, Bonev AD, Knot HJ, et al. Relaxation of arterial smooth muscle by calcium sparks. *Science.* 1995;270(5236):633-7.
18. Knot HJ, Standen NB, and Nelson MT. Ryanodine receptors regulate arterial diameter and wall [Ca2+] in cerebral arteries of rat via Ca2+-dependent K+ channels. *J Physiol.* 1998;508 (Pt 1):211-21.
19. Jackson WF. Potassium Channels in Regulation of Vascular Smooth Muscle Contraction and Growth. *Adv Pharmacol.* 2017;78:89-144.
20. Gonzales AL, Amberg GC, and Earley S. Ca2+ release from the sarcoplasmic reticulum is required for sustained TRPM4 activity in cerebral artery smooth muscle cells. *Am J Physiol Cell Physiol.* 2010;299(2):C279-88.
21. Dabertrand F, Kroigaard C, Bonev AD, Cognat E, Dalsgaard T, Domenga-Denier V, et al. Potassium channelopathy-like defect underlies early-stage cerebrovascular dysfunction in a genetic model of small vessel disease. *Proc Natl Acad Sci U S A.* 2015;112(7):E796-805.
22. Murray LS, Lu Y, Taggart A, Van Regemorter N, Vilain C, Abramowicz M, et al. Chemical chaperone treatment reduces intracellular accumulation of mutant collagen IV and ameliorates the cellular phenotype of a COL4A2 mutation that causes haemorrhagic stroke. *Hum Mol Genet.* 2014;23(2):283-92.
23. Malo A, Kruger B, Goke B, and Kubisch CH. 4-Phenylbutyric acid reduces endoplasmic reticulum stress, trypsin activation, and acinar cell apoptosis while increasing secretion in rat pancreatic acini. *Pancreas.* 2013;42(1):92-101.
24. Perlmutter DH. Chemical chaperones: a pharmacological strategy for disorders of protein folding and trafficking. *Pediatr Res.* 2002;52(6):832-6.
25. Hayashi G, Labelle-Dumais C, and Gould DB. Use of sodium 4-phenylbutyrate to define therapeutic parameters for reducing intracerebral hemorrhage and myopathy in Col4a1 mutant mice. *Dis Model Mech.* 2018;11(7).
26. Meuwissen ME, Halley DJ, Smit LS, Lequin MH, Cobben JM, de Coo R, et al. The expanding phenotype of COL4A1 and COL4A2 mutations: clinical data on 13 newly identified families and a review of the literature. *Genet Med.* 2015;17(11):843-53.
27. Shi Y, and Wardlaw JM. Update on cerebral small vessel disease: a dynamic whole-brain disease. *Stroke Vasc Neurol.* 2016;1(3):83-92.
28. Kraeuter AK, Guest PC, and Sarnyai Z. The Y-Maze for Assessment of Spatial Working and Reference Memory in Mice. *Methods Mol Biol.* 2019;1916:105-11.
29. Wenceslau CF, McCarthy CG, Earley S, England SK, Filosa JA, Goulopoulou S, et al. Guidelines for the measurement of vascular function and structure in isolated arteries and veins. *Am J Physiol Heart Circ Physiol.* 2021;321(1):H77-H111.
30. Harder DR. Pressure-dependent membrane depolarization in cat middle cerebral artery. *Circ Res.* 1984;55(2):197-202.

31. Knot HJ, and Nelson MT. Regulation of arterial diameter and wall [Ca2+] in cerebral arteries of rat by membrane potential and intravascular pressure. *J Physiol.* 1998;508 (Pt 1):199-209.
32. Pritchard HAT, Gonzales AL, Pires PW, Drumm BT, Ko EA, Sanders KM, et al. Microtubule structures underlying the sarcoplasmic reticulum support peripheral coupling sites to regulate smooth muscle contractility. *Sci Signal.* 2017;10(497).
33. Brayden JE, and Nelson MT. Regulation of arterial tone by activation of calcium-dependent potassium channels. *Science.* 1992;256(5056):532-5.
34. Launay P, Fleig A, Perraud AL, Scharenberg AM, Penner R, and Kinet JP. TRPM4 is a Ca2+-activated nonselective cation channel mediating cell membrane depolarization. *Cell.* 2002;109(3):397-407.
35. Gonzales AL, Yang Y, Sullivan MN, Sanders L, Dabertrand F, Hill-Eubanks DC, et al. A PLCgamma1-dependent, force-sensitive signaling network in the myogenic constriction of cerebral arteries. *Sci Signal.* 2014;7(327):ra49.
36. Earley S, Straub SV, and Brayden JE. Protein kinase C regulates vascular myogenic tone through activation of TRPM4. *Am J Physiol Heart Circ Physiol.* 2007;292(6):H2613-22.
37. Pires PW, Ko EA, Pritchard HAT, Rudokas M, Yamasaki E, and Earley S. The angiotensin II receptor type 1b is the primary sensor of intraluminal pressure in cerebral artery smooth muscle cells. *J Physiol.* 2017;595(14):4735-53.
38. Yamasaki E, Thakore P, Krishnan V, and Earley S. Differential expression of angiotensin II type 1 receptor subtypes within the cerebral microvasculature. *Am J Physiol Heart Circ Physiol.* 2020;318(2):H461-H9.
39. Schleifenbaum J, Kassmann M, Szijarto IA, Hercule HC, Tano JY, Weinert S, et al. Stretch-activation of angiotensin II type 1a receptors contributes to the myogenic response of mouse mesenteric and renal arteries. *Circ Res.* 2014;115(2):263-72.
40. Yasuda N, Miura S, Akazawa H, Tanaka T, Qin Y, Kiya Y, et al. Conformational switch of angiotensin II type 1 receptor underlying mechanical stress-induced activation. *EMBO Rep.* 2008;9(2):179-86.
41. McPherson PS, Kim YK, Valdivia H, Knudson CM, Takekura H, Franzini-Armstrong C, et al. The brain ryanodine receptor: a caffeine-sensitive calcium release channel. *Neuron.* 1991;7(1):17-25.
42. Wray S, and Burdyga T. Sarcoplasmic reticulum function in smooth muscle. *Physiol Rev.* 2010;90(1):113-78.
43. Iannitti T, and Palmieri B. Clinical and experimental applications of sodium phenylbutyrate. *Drugs R D.* 2011;11(3):227-49.
44. Joutel A, Monet-Lepretre M, Gosele C, Baron-Menguy C, Hammes A, Schmidt S, et al. Cerebrovascular dysfunction and microcirculation rarefaction precede white matter lesions in a mouse genetic model of cerebral ischemic small vessel disease. *J Clin Invest.* 2010;120(2):433-45.
45. Nelson MT, and Quayle JM. Physiological roles and properties of potassium channels in arterial smooth muscle. *Am J Physiol.* 1995;268(4 Pt 1):C799-822.
46. McCarron JG, Craig JW, Bradley KN, and Muir TC. Agonist-induced phasic and tonic responses in smooth muscle are mediated by InsP(3). *J Cell Sci.* 2002;115(Pt 10):2207-18.

47. Shmygol A, and Wray S. Modulation of agonist-induced Ca2+ release by SR Ca2+ load: direct SR and cytosolic Ca2+ measurements in rat uterine myocytes. *Cell Calcium.* 2005;37(3):215-23.
48. Parekh AB, and Putney JW, Jr. Store-operated calcium channels. *Physiol Rev.* 2005;85(2):757-810.
49. Fernandez RA, Wan J, Song S, Smith KA, Gu Y, Tauseef M, et al. Upregulated expression of STIM2, TRPC6, and Orai2 contributes to the transition of pulmonary arterial smooth muscle cells from a contractile to proliferative phenotype. *Am J Physiol Cell Physiol.* 2015;308(8):C581-93.
50. Krishnan V, Ali S, Gonzales AL, Thakore P, Griffin CS, Yamasaki E, et al. STIM1-dependent peripheral coupling governs the contractility of vascular smooth muscle cells. *Elife.* 2022;11.
51. Potier M, Gonzalez JC, Motiani RK, Abdullaev IF, Bisaillon JM, Singer HA, et al. Evidence for STIM1- and Orai1-dependent store-operated calcium influx through ICRAC in vascular smooth muscle cells: role in proliferation and migration. *FASEB J.* 2009;23(8):2425-37.
52. Bravo-Sagua R, Parra V, Munoz-Cordova F, Sanchez-Aguilera P, Garrido V, Contreras-Ferrat A, et al. Sarcoplasmic reticulum and calcium signaling in muscle cells: Homeostasis and disease. *Int Rev Cell Mol Biol.* 2020;350:197-264.
53. Schroder M, and Kaufman RJ. The mammalian unfolded protein response. *Annu Rev Biochem.* 2005;74:739-89.
54. Lebeau PF, Platko K, Byun JH, and Austin RC. Calcium as a reliable marker for the quantitative assessment of endoplasmic reticulum stress in live cells. *J Biol Chem.* 2021;296:100779.
55. Yamamoto WR, Bone RN, Sohn P, Syed F, Reissaus CA, Mosley AL, et al. Endoplasmic reticulum stress alters ryanodine receptor function in the murine pancreatic beta cell. *J Biol Chem.* 2019;294(1):168-81.
56. Favor J, Gloeckner CJ, Janik D, Klempt M, Neuhauser-Klaus A, Pretsch W, et al. Type IV procollagen missense mutations associated with defects of the eye, vascular stability, the brain, kidney function and embryonic or postnatal viability in the mouse, Mus musculus: an extension of the Col4a1 allelic series and the identification of the first two Col4a2 mutant alleles. *Genetics.* 2007;175(2):725-36.
57. Pallast N, Diedenhofen M, Blaschke S, Wieters F, Wiedermann D, Hoehn M, et al. Processing Pipeline for Atlas-Based Imaging Data Analysis of Structural and Functional Mouse Brain MRI (AIDAmri). *Front Neuroinform.* 2019;13:42.
58. Dong HW. *Allen reference atlas : a digital color brain atlas of the C57Black/6J male mouse.* Hoboken, N.J.: Wiley; 2008.
59. Gonzales AL, Amberg GC, and Earley S. Ca2+ release from the sarcoplasmic reticulum is required for sustained TRPM4 activity in cerebral artery smooth muscle cells. *American journal of physiology Cell physiology.* 2010;299(2):C279-88.